Analysis of the Dynamics of Assembly and Structural Impact for a Histidine Tagged FGF1−1.5 nm Au Nanoparticle Bioconjugate

Joshua M. Kogot,[†] Alex M. Parker,[†] Jihun Lee,[‡] Michael Blaber,[‡] Geoffrey F. Strouse,*[,†] and Timothy M. Logan*[,†]

Department of Chemistry and Biochemistry and Kasha Laboratory Institute of Molecular Biophysics, and Department of Biomedical Sciences, College of Medicine, Florida State University, Tallahassee, Florida 32306. Received May 21, 2009; Revised Manuscript Received September 4, 2009

Whether assembling proteins onto nanoscale, mesoscopic, or macroscropic material surfaces, maintaining a protein's structure and function when conjugated to a surface is complicated by the high propensity for electrostatic or hydrophobic surface interactions and the possibility of direct metal coordination of protein functional groups. In this study, the assembly of a 1.5 nm CAAKA passivated gold nanoparticle (AuNP) onto FGF1 (human acidic fibroblast growth factor) using an amino terminal His_6 tag is analyzed. The impact of structure and time-dependent changes in the structural elements in FGF1and FGF1-heparin in the presence of the AuNP is probed by a molecular beacon fluorescence assay, circular dichroism, and NMR spectroscopy. Analysis of the results indicates that a time-dependent evolution of the protein structure without loss of FGF1 heparin binding occurs following the formation of the initial FGF1-AuNP complex. The time-dependent changes are believed to reflect protein sampling of the AuNP surface to minimize the free energy of the AuNP-FGF1 complex without impacting FGF1 function.

INTRODUCTION

With the use of nanomaterials for biological assays (*1*−*7*), the desire to develop robust linkages that possess adaptable chemistries to interface biological molecules with nanomaterials, yet have minimal structural impact on the protein, has become a rapidly growing area of interest. A plethora of assembly strategies exist, using cysteine or thiol modifications (*8*−*10*), botin−streptavidin interactions (*11, 12*), click chemistry (*13*), and transition metal mediated histidine binding (*14, 15*), to name a few of the typical approaches (*1, 16, 17*). Each of these strategies has advantages and disadvantages, but all of the strategies require engineering non-native sequences into the protein, a secondary metal ion mediator, or antibody−antigen recognition step to form the construct, thus limiting the ability to extrapolate the results to the broader recombinantly engineered proteins employed by the biological community. Many of the studies to date have assumed that the structural elements are marginally perturbed in the local site of binding correlating the structural changes to the effect of nanoparticle (NP) charge, NP structure, and the site of protein substitution (*9, 18, 19*). While studies have shown protein function (*18, 20*), there is a notable lack of studies that fully investigate the dynamic changes occurring to the protein construct during the nanomaterial−protein assembly. In analogy to formation of self-assembled monolayers of proteins onto a surface, engineering a linkage that does not perturb the protein structure is challenging since the profusion of interactions stemming from potential backbone and side chain interactions with the NP surface can lead to alteration of protein structure and thus to protein misfolding (*7, 21*−*25*) and a loss in protein function (*21, 24, 26*−*29*). As demonstrated in several phage display assays (*30, 31*) on metal and semiconductor surfaces, the surface-mediated exchange reactions are governed by the amino acid functional groups, as well as electrostatic and hydrophobic interactions with the side chain and backbone of the protein.

The hexa-histidine (His_6) modification is widely used by recombinant protein chemists because of its high affinity for metal chelation, thereby facilitating purification by Ni(II) chelation chromatography. Several groups, including our own, have explored the use of the His_6 tag for assembly onto NP surfaces (*15, 32*−*37*). Our earlier results on peptide assembly demonstrated that the His_6-tag allows for region-selective assembly of small peptides onto the surface of the 1.5 nm AuNP through formation of a Au−Nε imidazole bond (*37*). Here, we extend the use of the His_6 tag recombinantly engineered to the amino terminus of FGF1 (human acidic fibroblast growth factor) to form a AuNP-FGF1 construct in order to assess the structural and potential functional impact on the protein. FGF1 is an important protein that exhibits mitogenic (cell division) and angiogenic (wound healing) properties and has emerged as a candidate for revascularization strategies of cardiac muscle following ischemic events (*38*−*40*). FGF1 binds heparin on the surfaces of cells and can accommodate oligosaccharides of varying sizes in the positively charged heparin binding pocket (*41*), but requires at least an octasaccharide heparin for FGF receptor (FGFR) activation. In this study, we probe the time-dependent conformational changes of an FGF1 sym6ΔΔ mutant during the assembly of the protein onto a 1.5 nm AuNP passivated by CAAKA, a zwitterionic peptide passivant layer. The use of a zwitterionic passivant layer on the nanoparticle surface has been shown to decrease the likelihood of nonspecific interactions between the protein and AuNP (*9, 42*), which allows the passivating peptide to be displaced and the exchange of passivants to dominate the final assemblage. The FGF1 sym6ΔΔ mutant was used for this study rather than the native FGF1, since the mutant is more sensitive to competitive binding interactions due to a modest folding free energy ($\Delta G_f = -33.9$ kJ/mol, 8.1 kcal/mol) (*43*), yet exhibits increased thermal stability compared to wild-type FGF1. In addition, the lower

* Corresponding authors. G.F.S: strouse@chem.fsu.edu, 95 Chieftan Way, Dept. of Chemistry and Biochemistry, Tallahassee, FL 32306. T.M.L: tlogan@fsu.edu, 91 Chieftan Way, Institute of Molecular Biophysics, Tallahassee, FL 32306.

[†] Department of Chemistry and Biochemistry and Kasha Laboratory Institute of Molecular Biophysics.

[‡] Department of Biomedical Sciences, College of Medicine.

heparin binding affinity for the mutant will allow the impact of AuNP interactions with the protein to be assessed (*44*).

Analysis of the time-dependent changes in structure and function of FGF1 sym6ΔΔ and the heparin-bound analogue in the presence of the 1.5 nm AuNP is examined through the use of a combination of biophysical techniques, including CD, NMR, and molecular beacon kinetic assays, to assess the formation of the FGF1-AuNP conjugate. Observation of a time-dependent evolution of the FGF1structural elements over 18 h is observed and attributed to initial binding of FGF1 to AuNP at multiple locations on the protein surface followed by the more energetically favorable binding of the His_6 tail selectively to the AuNP surface. The time-dependent evolution is consistent with earlier results for peptide assembly onto a AuNP (*37*). The maintenance of structure and heparin binding ability for the FGF1 mutant confirms that the His_6 metal affinity tag (His-tag) used to enhance purification of recombinant proteins can be routinely utilized for site-specific assembly of recombinant proteins onto AuNP surfaces. The development of more robust methods for site-specific attachment that minimize nonspecific interactions while maintaining the structural integrity and functionality of a protein when appended to the surface of a nanometal is critical if these systems are to be used in biomedical technologies (*9, 10, 13, 45, 46*). Although not pursued in this study, region-selective coupling of the FGF1 without perturbation of the protein function may allow tracking FGF1 activity in cells via optical or electron microscopy methods.

Experimental Procedures. *Expression and Purification of sym6ΔΔ Mutant of Human FGF-1.* The amino-terminal His_6-tag (*47*) form of the sym6ΔΔ mutant of FGF-1 (*44*) (for simplicity referred to here as FGF1) was expressed and purified according to published procedures (*47*−*49*). Briefly, clarified cell lysate was purified by nickel affinity chromatography (HisPrep FF 16/10 column, GE Biosciences) followed by size exclusion chromatography (Superdex75 10/300 GL column, GE Biosciences). U-^{15}N-FGF was grown in M9 media with $(^{15}NH_4)_2SO_4$ as the sole nitrogen source and purified as above. FGF1-heparin complexes were formed by incubating low molecular weight heparin sodium salt (Sigma) with an equimolar solution of FGF1 for 30 min prior to all experiments.

Preparation of Au-CAAKA and Au-CAAKA-FITC. Au nanoparticles (1.5 nm AuNP) were passivated initially with triphenylphosphine (TPP) in toluene (*50*) and then ligand-exchanged with a zwitterionic peptide (CAAKA) to yield a water-soluble CAAKA-AuNP. The Au particle size was confirmed by electron microscopy and by UV−vis, noting the absence of a plasmon resonance at 520 nm, typically observed for AuNPs greater than 2.5 nm in diameter. For molecular beacon studies, CAAKA was labeled with fluorescein 5-isothiocyanate (FITC) (Sigma) through the lysine amine according to manufacturer instructions and purified by HPLC (C_{18}-RP) before being exchanged onto the AuNP.

Molecular Beacon Assay of FGF1 Assembly onto AuNP Surface. FGF1 or FGF1−heparin were exchanged onto Au-CAAKA-FITC in 50 mM sodium phosphate, 10 mM $(NH_4)_2SO_4$, 100 mM NaCl, pH = 7.5 (Buffer A), at a 1:1 protein to AuNP (1 μM) ratio at 25 °C. Exchange was monitored at 7 min intervals over an 18 h period using a nanometal surface energy transfer (NSET) (*51*) based molecular beacon assay based on dequenching of CAAKA-FITC fluorescence upon release from AuNP. The fluorescence spectra were collected from 300 to 600 nm in triplicate on a Cary Eclipse (Varian) in 1 cm path length cell (100 μL total volume) at 25 °C in Buffer A.

Time-Dependent Structural Changes in FGF1 by CD Spectroscopy. Circular dichroism (CD) spectra were collected between 190 and 260 nm with 0.5 nm steps and 1 s signal averaging on an AVIV 202 CD spectrometer at 25 °C in Buffer A using a 1 cm path length cell. Each sample, including buffer, was measured in triplicate and averaged before buffer subtraction. Sample concentrations were typically 5 μM FGF1 and/or 5 μM Au-CAAKA. The secondary structure content of FGF1 sym6ΔΔ mutant was analyzed in the CD spectra using *CDPro* software (*52*).

2D HSQC NMR Analysis of Protein Structural Perturbations. 2D-^{1}H,^{15}N HSQC experiments were performed on U-^{15}N-FGF1 on a Varian Inova spectrometer operating at 11.74T (Varian Inc., Palo Alto, CA). Protein concentrations were typically 200 μM in 100 mM phosphate, 200 mM $(NH_4)_2SO_4$, 100 mM NaCl at pH = 6.0 (Buffer B). HSQC spectra were collected over 8333 Hz (1500 Hz) and digitized by 1024 (220) complex points in the ^{1}H (^{15}N) dimensions in 16 scans per t_1 increment for a total data collection time of ∼45 min. Data collection for each HSQC spectrum was initiated at 0, 5, and 18 h following addition of Au-CAAKA. Data were processed with zero-filling to yield a final digital resolution of 4 and 15.7 Hz in ^{1}H and ^{15}N dimensions, respectively. Data processing was performed using NMRPipe and analyzed using NMR-View (*53*). Changes in resonance position ($\Delta\delta$) upon addition of CAAKA-Au were quantified as $\Delta\delta = [(\delta H)^2 + (\delta N/6)^2]^{1/2}$ (*54*).

RESULTS

Following secretion from the cell, FGF1 binds to heparin and the FGF1-heparin complex is then recognized by the FGF receptor to initiate signaling (*55*). Heparin has a net negative charge, and electrostatic interactions between heparin and the protein binding pocket impact the binding affinity of heparin to FGF1. A structural model indicating residue location and the electrostatic potential at physiological pH of FGF1 sym6ΔΔ is presented in Figure 1. The amino-terminal His_6-tag should minimally perturb the protein structure and, more importantly, the heparin binding pocket, as the His_6-tag will position the AuNP on the side of FGF1 opposite the heparin binding pocket. The assembly of the FGF1 onto the AuNP is expected to occur via a surface-mediated ligand exchange reaction of the CAKKA peptide passivant shell appended to the AuNP by the formation of the Nε imidazole−Au interaction. The presence of the roughly 2 nm positively charged heparin binding pocket on FGF1 increases the potential for deleterious interactions between the protein and the 1.5 nm AuNP, and thus, the hypoactive form of FGF1 (sym6ΔΔ mutant) is the ideal test case for assessing potential loss of protein activity in the presence of the AuNP.

To minimize potential heparin binding pocket interactions, the 1.5 nm AuNP is passivated with the zwitterionic peptide sequence CAKKA (Cys-Ala-Lys-Lys-Ala) (*9, 42*). The CAAKA peptide is ligated to the AuNP via a Au-*S* interaction via the reduced Cys (C) amino acid. Fluorescent labeling of the CAAKA passivant by FITC (fluorescein) appended to the Lys (K) allows the recovery of FITC photoluminescence (PL) to be used as a probe of CAAKA displacement from the surface of the AuNP. When the CAAKA-FITC fluorogenic agent is appended to the AuNP, the FITC PL is quenched via energy transfer (*51, 56*).

In Figure 2, displacement of the CAAKA-FITC passivant from the AuNP surface by FGF1 binding is observed to result in the onset of FITC PL. The loss of the CAAKA-FITC passivant (onset of FITC PL) from the AuNP exhibits bimodal kinetics for both the addition of FGF1 and FGF1-heparin to the 1.5 nm Au-CAAKA-FITC construct (Figure 2). No time-dependent optical changes in the Au-CAAKA-FITC construct are observed in the absence of added protein (not shown). The bimodal trajectory in Figure 2 is verified by *F*-statistics through the analysis of χ^2 by fitting a series of functions with increasing number of exponentials. Fitting to a single exponential resulted in large χ^2 values which were significantly reduced in a

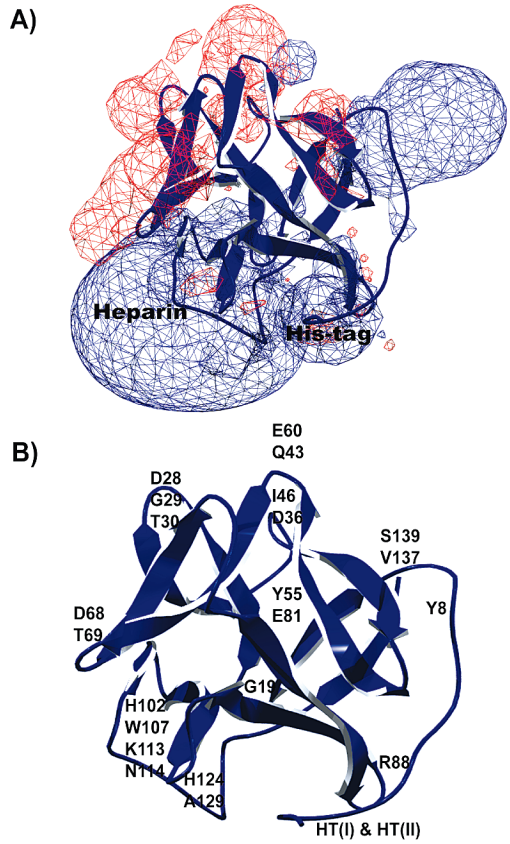

Figure 1. FGF1 crystallographic structure model (PDB ID: 1RG8) showing (A) an electrostatic surface potential model for FGF1 with the heparin binding region and His-tag region and (B) FGF1 structure with labeled key residues using the single letter code for the amino acids and the numbering for amino acid sequence.

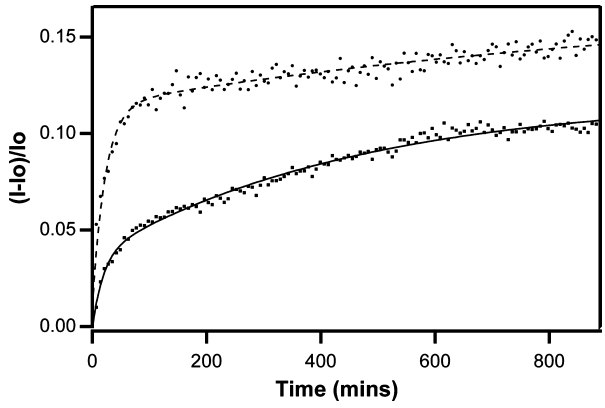

Figure 2. FGF1 and FGF1-heparin FITC PL intensity for the CAAKA-FITC displacement on the 1.5 nm AuNP surface byFGF1 (solid) and FGF1-heparin (dash). The PL intensity is monitored at 520 nm.

biexponential fit; fitting to a triexponential function did not significantly improve the quality of the fit according to the *F*-statistic.

Table 1 lists the experimentally fit rates and amplitudes for release of CAAKA-FITC upon addition of FGF1 or FGF1-heparin. The observed fast and slow rates are quite similar, within a factor of 2 for FGF1 and FGF1-heparin. However, the contribution to the total intensity recovery is reversed, with FGF1-heparin exhibiting higher amplitude for the fast phase, while FGF1 shows higher amplitude for the slow phase. The difference in rate and amplitude for CAAKA-FITC release between the FGF1 and the FGF1-heparin complex is intriguing and may reflect the fewer sampling configurations available for

Table 1. Calculated Rate and Amplitude Values for the Release of CAAKA-FITC from the Surface of a 1.5 nm AuNP when Treated withFGF1 or FGF1-Heparin

	fast phase		slow phase	
	rate (min^{-1})	amplitude (%)	rate (min^{-1})	amplitude (%)
FGFI	0.0532(0.0080)	23	0.0022(0.0002)	77
FGFI heparin	0.0446(0.0036)	67	0.0009(0.0005)	33

the heparin-bound FGF1 relative to FGF1 when interacting with the AuNP surface. The loss of conformational freedom arising from the binding of heparin to FGF1 eliminates the positive heparin binding pocket and reduces the conformational dynamics of the FGF1, which could lead to the observed differences in the rate of structural minimization for the two forms of FGF1.

The FITC intensity trajectories in Figure 2 have not reached an asymptotic value within the time scale of the experiment, although extrapolation of the data to time infinity implies that both systems will achieve similar asymptotic values. The observed FITC PL recovery for FGF1 after 15 h is ~9% and ~14% for FGF1-heparin. Assuming a loading level of approximately 40 CAAKA-FITC based on the analysis of passivant exchange on AuNPs by Woehrle et al. (*57*), the displacement corresponds to between four and six CAAKA-FITC peptide passivants from the AuNP surface, four in the case of FGF and six in the case of FGF1-heparin. Assuming the peptide displacement results from one His residue interacting with the NP surface, this yields one protein per AuNP, which is consistent with our previous report of a single His_6 peptide binding to a AuNP (*37*).

Further evidence of a strong bonding interaction between the AuNP and the FGF1 is provided by chromatographic analysis using size exclusion and PAGE electrophoresis (Supporting Information Figures 1 and 2). Upon addition of FGF1 to a solution of AuNP in a 10:1 mol ratio, loss of the original sharp AuNP signal is observed by size exclusion analysis in Superdex75 after 1 h of mixing the AuNP and FGF1 (Supporting Information Figure 1). The signal loss in FGF1 is correlated with the appearance of a new broad feature at shorter retention time. The decrease in the FGF1 band is approximately 10% (~90% unchanged) for identical concentrations of FGF1, indicating approximately a 1:1 binding ratio. The broad feature for the AuNP-FGF1 assembly appears to have multiple components that could not be separated and is believed to reflect more than one binding motif at this short mixing time (1 h). The assumption from the optical assay for the FGF1-AuNP assembly having not fully evolved to the final structural conformation based on the biexponential rise time of the signal is consistent with the size-exclusion results. Further evidence of chromatographic stability is provided by Native-PAGE analysis of a 1: 1 ratio of FGF1 to AuNP (Supporting Information Figure 2). In the native PAGE, no free FGF1 is observed after treatment with the AuNP as evidenced by the lack of Coomassie blue stained FGF1 protein (lanes 4 and 7, Supporting Information Figure 2B). In addition, a slight mobility shift is observed for the AuNP due to the mobility difference of the FGF1-AuNP complex (lanes 4 and 7, Supporting Information Figure 2A). The small shift in the mobility between the AuNP and FGF1-AuNP and FGF1 (sane 3 vs 4) and the FGF1-heparin-AuNP (lane 3 vs 7) is consistent with the AuNP creating a strong assembly with the FGF1 protein.

Evidence of Structural Perturbation of FGF1 in the Presence of the AuNP. On the basis of the electrostatic map in Figure 1, the possibility that protein sampling gives rise to the observed dynamics is not surprising. The possibility for electrostatic and hydrophobic interactions can impact the secondary structure as well. In Figure 3, the CD spectrum of FGF1 prior to addition of the AuNP, 15 min, 6 h, and 24 h

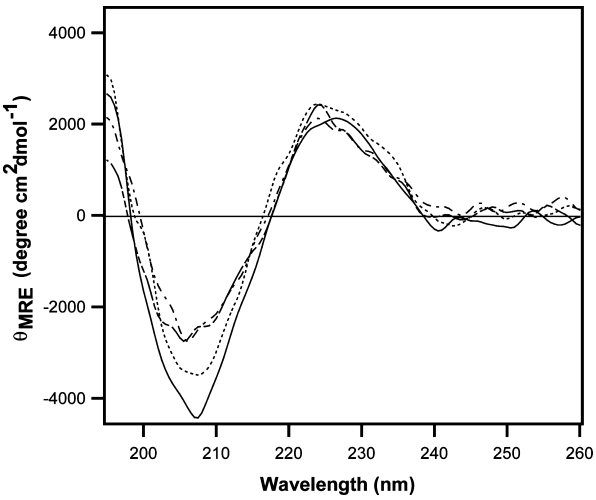

Figure 3. Circular dichroism spectra of FGF1 (—) and changes at 15 min (••••), 6 h (----), and 24 h (-•-) following the addition of Au-CAAKA to the FGF1 solution.

following addition of equimolar AuNP is shown. FGF1-heparin was not analyzed by CD spectroscopy.

The secondary structure of FGF1 are composed of β-sheet, β-turn, random coil, and α-helix character based upon crystallography and analysis by *CDPro* (*52*) fitting of the CD spectra. Using *CDPro* software, in the absence of the AuNP, FGF1 contains 35% β-sheet and 25% β-turn, with the remaining 40% attributed to random coil and α-helix character. Following addition of AuNP to FGF1, the 207 nm negative phase signal, which likely arises from a combination of α-helix and β-sheet signals, exhibits a loss of intensity during the first 6 h. The positive CD signal maximum at 230 nm, arising from β-turn, exhibits no substantial change over the entire experimental time domain. Analyzing the signal change in the presence of the AuNP indicates that a 10% increase in β-sheet and a 7% decrease in β-turn content occur for the FGF1−AuNP conjugate during the first 6 h, with minimal subsequent structural perturbations observed relative to the native FGF1 structure at longer experimental times.

A more detailed picture of the structural perturbations of FGF1 upon binding to the AuNP can be analyzed by 2D NMR when the experimental data for CAAKA-FITC release and the CD spectra suggest the FGF1-AuNP has approached a structural minimum. Inspection of the NMR data at 22 min (Supporting Information Figure 3) and 6 h (Supporting Information Figure 4) is intriguing but complicated by the fact that the structure is still evolving and thus exhibits more global changes in the protein; therefore, the discussion below is limited to the data obtained at 18 h exposure times (Figure 4) to simplify data interpretation.

Figure 4A shows the HSQC spectrum of FGF1 in the absence of the AuNP (cyan) and 18 h following addition of the AuNP (magenta). Comparison of the 2D NMR plots indicates that the vast majority of the residues of FGF1 are minimally impacted with the exception of the His_6-tag residues HT(I) and HT(II). The two resonances assigned, HT(I) and HT(II), are not observable immediately after exposure to the AuNP. Whether these changes in resonance intensity arise from altered conformational exchange or a true increase in transverse relaxation rates cannot be determined from these spectra. In addition, subtle changes are observable for the individual intensity and protein resonances following FGF1 interaction with the AuNP, particularly for protein residues in or near the His_6-tag region (Figure 1). S139 shows significantly lower resonance intensity 18 h after addition of AuNP (Figure 4B), whereas H124 and E60 show changes in resonance frequency with little affect on intensity. In general, the same residue changes for the 6 h time point are observed, but in addition, G19, V55, and I25 also show chemical shift changes (Supporting Information Figure 4). The intensity and resonance changes clearly indicate these residues are significantly impacted by addition of the AuNP.

Greater insight into the changes occurring at the individual protein residues in the presence of the AuNP can be deduced by plotting the change in chemical shift ($\Delta\delta$) in the HSQC experiment for individual protein residues relative to FGF1 in the absence of the AuNP (Figure 5) at 18 h and 6 h (Supporting Information Figure 5). Residues showing $\Delta\delta \geq 20$ Hz (digital resolution = 8.3 Hz on this scale) are considered significant and are labeled in the $\Delta\delta$ plot with their single letter abbreviation at position in the protein (Figure 1). A residue showing >100 Hz shift or a complete loss of intensity is artificially shown in the $\Delta\delta$ plot as a negative value.

The $\Delta\delta$ plots indicate that residues G19, E60, and H102, which are related structurally by the threefold symmetry of the FGF1 β-trefoil (*55*), along with Q43 and H124 show the largest chemical shift change between the protein in the presence and absence of the AuNP. The changes in the residue intensity and frequency are apparent at the earliest time point (22 min) and remain relatively constant through the 18 h time point (Figure 5). Residue G19 also shows a significant change, although a

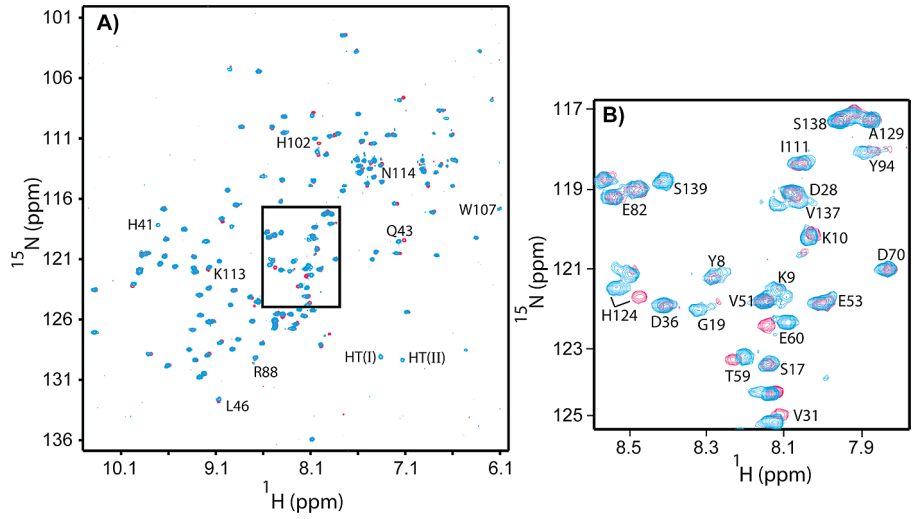

Figure 4. (A) $^1H-^{15}N$ HSQC NMR spectrum of FGF1 (cyan) and FGF1-AuNP (magenta) at 18 h. (B) Expanded representative region of HSQC spectra highlighting chemical shift changes, peak loss, and no change for FGF1-AuNP at 18 h postincubation.

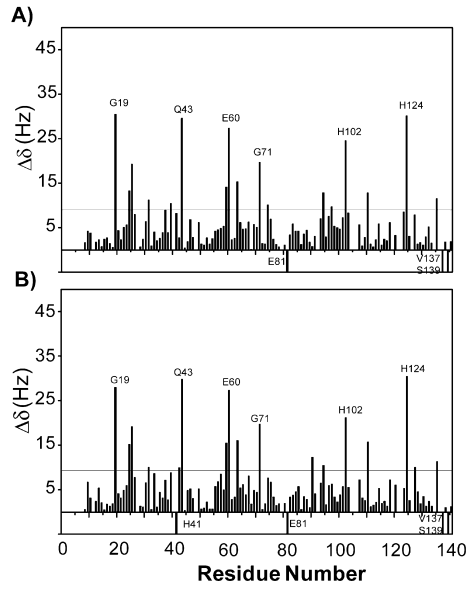

Figure 5. Δδ plot showing chemical shift differences and peak intensity loss (negative intensity) (A) 22 min and (B) 18 h incubation of FGF1 sym6ΔΔ with a 1.5 nm CAAKA passivated AuNP.

weak resonance G19 has a large shift in frequency implying that a structural perturbation may arise upon binding of the AuNP.

Residues H41, E81, V137, and S139 are not observed following the addition of AuNP and are represented as negative values in Figure 5. The signal loss for H41 may not be significant, as the loss of the resonance signal may reflect the weak native intensity observed for H41 in the FGF1 NMR spectra in the absence of the AuNP. However, the loss of E81, V137, and S139 is significant, as these are strong resonances in the FGF1 NMR spectra, implying that either a large frequency shift or a drastic change in dynamics for these residues occurs upon interaction of FGF1 with the AuNP. Residue E81 is located in close proximity to the His_6-tag region and changes in V137 and S139 are not surprising, since the C-terminal β-strand region is unstructured in both the His_6-tag (PDB accession 1JQZ or high-resolution 1RG8) and non-His_6-tag form of FGF1 (PDB accession 2AFG) and has a β-sheet interaction with the N-terminus β-strand. Changes in the N-terminal β-strand near the His_6-tag may indicate either ordering or disordering of the C-terminus β-strand upon AuNP binding.

Investigation of Heparin Binding in Presence of AuNP. NMR and crystallographic evidence for FGF1 binding with heparin suggest that heparin binding occurs through interactions with residues between G110-G120 and R122-A129, with large effects seen for residues K113 and K118 (*38, 40, 58*). On the basis of analysis of the NMR data for the FGF1-AuNP construct, the structural perturbations in FGF1 appear to be localized in the His_6-tag region and possibly the heparin binding pocket, which may potentially impact the heparin binding affinity. It is worth noting that changes in NMR resonances do occur in regions distal from the site of binding. For instance, it is well-known that heparin binding affects residues outside the heparin binding pocket (*40*).

A Δδ plot for heparin bound to FGF1 sym6ΔΔ in the absence of the AuNP calculated from the $^1H-^{15}N$ HSQC at 6 h (Supporting Information Figure 6) shows resonance and intensity perturbations for residues G19, D36, H42, R88, W107, K113, N114, and I130 (Figure 6B) in good agreement with previously reported NMR results on wild-type FGF1 (*38, 40, 58*). Comparison of the Δδ NMR plot derived from the $^1H-^{15}N$ HSQC spectra (Figure 6A) for adding heparin to FGF1 in the

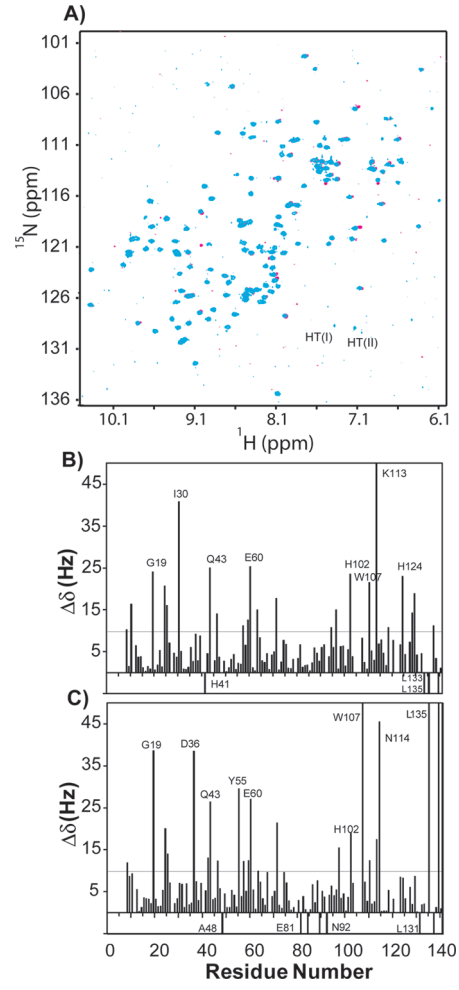

Figure 6. (A) $^1H-^{15}N$ HSQC NMR spectrum of FGF1 (cyan) and FGF1-heparin-AuNP (magenta) at 18 h. (B) Δδ plot showing chemical shift changes and loss of intensity (negative value) for (C) FGF1 with heparin and (B) FGF1 with heparin and AuNP after 18 h incubation.

presence and absence of AuNP (Figure 6C) shows similar perturbations as when AuNP is added to FGF1 in the presence and absence of heparin, indicating that the AuNP does not compete with heparin binding. Namely, residues W107, G110, K113, and N114 are impacted in the heparin−FGF1 alone and also show similar perturbations for the AuNP heparin−FGF1. In addition, residues A48, E81, L84, L89, and N92 show a complete intensity loss after 18 h with heparin and the AuNP (indicated as a negative value in Figure 4B), which is not observed in the absence of the AuNP. The loss of intensity of residues L89 and N92 is not surprising, since these residues are located in close proximity to the His_6-tag region in a flexible β-turn that has been shown to adopt significantly different structural conformations in FGF1/FGFR complexes (*59, 60*). The AuNP-specific changes are similar to those observed for FGF1 assembly onto the AuNP in the absence of heparin. Thus, the observation that a number of residues that are impacted only if the AuNP is present, including HT(I), HT(II), Y55, V137, and S139, and residues specific for experiments with heparin binding to FGF1 such as W107, G110, K113, and N114 also have chemical shift differences compared to FGF1 alone further confirms that both the AuNP and heparin remain bound after 18 h.

DISCUSSION

Our results show a strong time dependence for FGF1−AuNP complex formation. Correlating the changes observed in

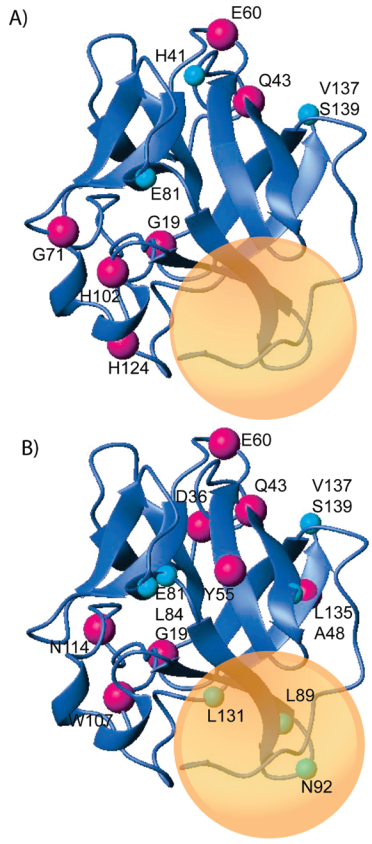

Figure 7. FGF1 crystallographic structure model (PDB ID: 1RG8) showing residues that exhibit chemical shift change (magenta), intensity differences (cyan), and His-tag (gold) affected by AuNP binding after 18 h for (A) FGF1 and (B) FGF1-heparin. The AuNP is overlaid in the His_6-tag region and does not represent a cocrystallized structure.

the NMR spectra for FGF1 and FGF1−heparin in the presence of the AuNP allows a model to be drawn indicating the regions of proposed AuNP interactions. Figure 7 shows the position of FGF1 residues that are most strongly affected by addition of AuNP after 18 h. Magenta balls indicate the position of backbone amides showing the largest $\Delta\delta$ values, and cyan indicates the positions of largest resonance intensity change. In addition to the residues of the His_6-tag, AuNP binding affects residues in β-turn regions, with little impact on β-sheet residues. A comparison of the affected residues (large or small) indicates that AuNP effects are noted in both positive and negative charge regions, and could be due to both nonspecific electrostatic interactions or motional dynamic changes, which are often seen with FGF1 flexibility changes upon heparin binding (*40*). The number and location of residues affected by AuNP binding in the NMR results are consistent with the relatively modest changes in secondary structure detected by CD. Importantly, the heparin binding pocket on the FGF1 remains largely unaffected by the AuNP binding, although the E81 residue (a surface residue in close spatial proximity to the His_6-tag region) is affected by AuNP binding. Comparison of the binding of FGF1-sym6ΔΔΔ in the absence of the His_6-tag could not be carried out due to the poor expression level and stability of FGF1 in the absence of the His_6 tag (*43*).

The bimodal kinetics for CAAKA release during the FGF1 assembly onto the AuNP can be attributed to one of two simple models, which may not be mutually exclusive. In one model, the bimodal nature of CAAKA-FITC release upon FGF binding reflects His_6-tag binding directly to readily accessible vertices and edges of the AuNP (*61, 62*) followed by slower release of CAAKA-FITC due to steric clash with the assembled FGF1. The zwitterionic CAAKA surface ligand is likely to minimize the nonspecific interactions, but given the degree of both positive and negative surface regions (Figure 1), electrostatic interactions between FGF1 and AuNP likely are inevitable. Alternatively, the bimodal kinetics may represent a rapid but nonspecific adsorption of FGF1 onto the AuNP followed by a slow rearrangement toward the more stable binding through the His_6-tag. The higher initial rate of assembly for FGF1−heparin would then reflect the fact that the His_6-tag is more favorable for binding than in FGF1 alone, or that the bound heparin eliminates some of the nonspecific adsorption by blocking the large positive charge region near the His_6-tag (Figure 1). Regardless of the mechanistic pathway for assembly, both models suggest an evolving interaction driven by protein sampling of the AuNP surface leading to a stable complex that minimally perturbs protein secondary structure or biological function by positioning the heparin binding pocket away from the His_6-tag-driven AuNP surface-mediated assemblage.

The correlation of the molecular beacon, gel electrophoresis, NMR, and CD spectroscopies supports a conclusion that the His_6-tag is the dominant interaction with the AuNP surfaces at long incubation times leading to small perturbations on the global FGF1 structure. The assembly arises from peptide displacement by the His residue leading to a His (Nε)-Au coordination. While it is surprising that the thiol (cys-) functionality is displaced by the His residue since thiols are strong coordinators of Au surfaces, the strong association of the His_6-tag reflects the enhanced thermodynamic stability for the His_6 residue arising from the multichelate effect, a common observation for metal−liagnd stabilization in metal coordination chemistry (*63*−*65*). The slow dynamics of assembly reflects minimization of the protein AuNP conjugate as the protein samples the AuNP surface. The ability to bind a AuNP to His_6-tag proteins opens another interfacial bridge between biology and nanoscience. This structure/function study of FGF1-AuNP binding provides evidence of stable, direct protein−Au conjugation without loss of normal function. The His_6-tag FGF1 sym6ΔΔ binding to the AuNP is stable in size-exclusion chromatography (Supporting Information Figure 1) and PAGE analysis (Supporting Information Figure 2) further confirming the suitability of the His_6-tag as a robust, stable linkage to a AuNP. This study enables further use of AuNP with recombinant His-tag proteins for intracellular delivery, biophysical studies, sensing, imaging, and other nanobiomedical applications.

ACKNOWLEDGMENT

The authors would like to thank Dr. Claudius Mundoma, Director of the Physical Biochemistry Facility in the Institute of Molecular Biophysics at Florida State, for help with circular dichroism measurements. The authors would also like to thank Dr. Tom Gedris and Steve Freitag in the NMR facility in the Department of Chemistry and Biochemistry at Florida State University. This work was supported by NIH NBIB-R0EB000832 (GFS) and NIH AI-R01021628 (TML).

Supporting Information Available: (SF1) Size-exclusion chromatography of FGF1:AuNP (10:1); (SF2) Native PAGE gel of FGF1:AuNP (1:1); (SF3) HSQC spectra for FGF1-FGF-AuNP (22 min); (SF4) HSQC spectra for FGF1-FGF1-AuNP (6 h); (SF5) FGF1 and FGF1-AuNP $\Delta\delta$ plot 6 h incubation time; (SF6) HSQC spectra for FGF1-FGF1-heparin at 18 h. This material is available free of charge via the Internet at http://pubs.acs.org.

LITERATURE CITED

(1) Medintz, I. L., Uyeda, H. T., Goldman, E. R., and Mattoussi, H. (2005) Quantum dot bioconjugates for imaging, labelling and sensing. *Nat. Mater. 4*, 435–446.

(2) Gao, X. H., Yang, L. L., Petros, J. A., Marshal, F. F., Simons, J. W., and Nie, S. M. (2005) In vivo molecular and cellular imaging with quantum dots. *Curr. Opin. Biotechnol. 16*, 63–72.

(3) Fritzsche, W., and Taton, T. A. (2003) Metal nanoparticles as labels for heterogeneous, chip-based DNA detection. *Nanotechnology 14*, R63–R73.

(4) Porta, F., Speranza, G., Krpetic, Z., Dal Santo, V., Francescato, P., and Scari, G. (2007) Gold nanoparticles capped by peptides. *Mater. Sci. Eng., B 140*, 187–194.

(5) You, C. C., De, M., and Rotello, V. M. (2005) Monolayer-protected nanoparticle-protein interactions. *Curr. Opin. Chem. Biol. 9*, 639–46.

(6) Chan, W. C., Maxwell, D. J., Gao, X., Bailey, R. E., Han, M., and Nie, S. (2002) Luminescent quantum dots for multiplexed biological detection and imaging. *Curr. Opin. Biotechnol. 13*, 40–6.

(7) Chah, S., Hammond, M. R., and Zare, R. N. (2005) Gold nanoparticles as a colorimetric sensor for protein conformational changes. *Chem. Biol. 12*, 323–328.

(8) Krpetic, Z., Nativo, P., Porta, F., and Brust, M. (2009) A Multidentate peptide for stabilization and facile bioconjugation of gold nanoparticles. *Bioconjugate Chem. 20*, 619–624.

(9) Aubin-Tam, M. E., and Hamad-Schifferli, K. (2005) Gold nanoparticle-cytochrome C complexes: the effect of nanoparticle ligand charge on protein structure. *Langmuir 21*, 12080–4.

(10) Becker, C. F. W., Marsac, Y., Hazarika, P., Moser, J., Goody, R. S., and Niemeyer, C. M. (2007) Functional immobilization of the small GTPase Rab6A on DNA-gold nanoparticles by using a site-specifically attached poly(ethylene glycol) linker and thiol place-exchange reaction. *ChemBioChem 8*, 32–36.

(11) Weiss, B., Schneider, M., Muys, L., Taetz, S., Neumann, D., Schaefer, U. F., and Lehr, C. M. (2007) Coupling of biotin-(poly(ethylene glycol))amine to poly(D,L-lactide-co-glycolide) nanoparticles for versatile surface modification. *Bioconjugate Chem. 18*, 1087–94.

(12) Ackerson, C. J., Jadzinsky, P. D., Jensen, G. J., and Kornberg, R. D. (2006) Rigid, specific, and discrete gold nanoparticle/antibody conjugates. *J. Am. Chem. Soc. 128*, 2635–2640.

(13) Brennan, J. L., Hatzakis, N. S., Tshikhudo, T. R., Dirvianskyte, N., Razumas, V., Patkar, S., Vind, J., Svendsen, A., Nolte, R. J. M., Rowan, A. E., and Brust, M. (2006) Bionanoconjugation via click chemistry: The creation of functional hybrids of lipases and gold nanoparticles. *Bioconjugate Chem. 17*, 1373–1375.

(14) Abad, J. M., Mertens, S. F., Pita, M., Fernandez, V. M., and Schiffrin, D. J. (2005) Functionalization of thioctic acid-capped gold nanoparticles for specific immobilization of histidine-tagged proteins. *J. Am. Chem. Soc. 127*, 5689–94.

(15) Medintz, I. L., Clapp, A. R., Mattoussi, H., Goldman, E. R., Fisher, B., and Mauro, J. M. (2003) Self-assembled nanoscale biosensors based on quantum dot FRET donors. *Nat. Mater. 2*, 630–8.

(16) Aubin-Tam, M. E., and Hamad-Schifferli, K. (2008) Structure and function of nanoparticle-protein conjugates. *Biomed. Mater. 3*, 034001.

(17) You, C. C., Verma, A., and Rotello, V. M. (2006) Engineering the nanoparticle-biomacromolecule interface. *Soft Matter 2*, 190–204.

(18) Aubin-Tam, M. E., Hwang, W., and Hamad-Schifferli, K. (2009) Site-directed nanoparticle labeling of cytochrome c. *Proc. Natl. Acad. Sci. U.S.A. 106*, 4095–100.

(19) Verma, A., Nakade, H., Simard, J. M., and Rotello, V. M. (2004) Recognition and stabilization of peptide alpha-helices using templatable nanoparticle receptors. *J. Am. Chem. Soc. 126*, 10806–7.

(20) Niemeyer, C. M. (2003) Functional hybrid devices of proteins and inorganic nanoparticles. *Angew. Chem., Int. Ed. Engl. 42*, 5796–800.

(21) Staii, C., Wood, D. W., and Scoles, G. (2008) Verification of biochemical activity for proteins nanografted on gold surfaces. *J. Am. Chem. Soc. 130*, 640–646.

(22) Blum, A. S., Soto, C. M., Wilson, C. D., Brower, T. L., Pollack, S. K., Schull, T. L., Chatterji, A., Lin, T. W., Johnson, J. E., Amsinck, C., Franzon, P., Shashidhar, R., and Ratna, B. R. (2005) An engineered virus as a scaffold for three-dimensional self-assembly on the nanoscale. *Small 1*, 702–706.

(23) Soto, C. M., Blum, A. S., Wilson, C. D., Lazorcik, J., Kim, M., Gnade, B., and Ratna, B. R. (2004) Separation and recovery of intact gold-virus complex by agarose electrophoresis and electroelution: Application to the purification of cowpea mosaic virus and colloidal gold complex. *Electrophoresis 25*, 2901–2906.

(24) Calabretta, M. K., Matthews, K. S., and Colvin, V. L. (2006) DNA binding to protein-gold nanocrystal conjugates. *Bioconjugate Chem. 17*, 1156–1161.

(25) Hu, Y., Das, A., Hecht, M. H., and Scoles, G. (2005) Nanografting de novo proteins onto gold surfaces. *Langmuir 21*, 9103–9109.

(26) Bayraktar, H., You, C. C., Rotello, V. M., and Knapp, M. J. (2007) Facial control of nanoparticle binding to cytochrome c. *J. Am. Chem. Soc. 129*, 2732−+.

(27) Ao, L. M., Gao, F., Pan, B. F., Cui, D. X., and Gu, H. C. (2006) Interaction between gold nanoparticles and bovine serum albumin or sheep antirabbit immunoglobulin G. *Chin. J. Chem. 24*, 253–256.

(28) Aubin, M. E., Morales, D. G., and Hamad-Schifferli, K. (2005) Labeling ribonuclease S with a 3 nm Au nanoparticle by two-step assembly. *Nano Lett. 5*, 519–22.

(29) Brewer, S. H., Glomm, W. R., Johnson, M. C., Knag, M. K., and Franzen, S. (2005) Probing BSA binding to citrate-coated gold nanoparticles and surfaces. *Langmuir 21*, 9303–9307.

(30) Whaley, S. R., English, D. S., Hu, E. L., Barbara, P. F., and Belcher, A. M. (2000) Selection of peptides with semiconductor binding specificity for directed nanocrystal assembly. *Nature 405*, 665–8.

(31) Peelle, B. R., Krauland, E. M., Wittrup, K. D., and Belcher, A. M. (2005) Design criteria for engineering inorganic material-specific peptides. *Langmuir 21*, 6929–33.

(32) Kroger, D., Liley, M., Schiweck, W., Skerra, A., and Vogel, H. (1999) Immobilization of histidine-tagged proteins on gold surfaces using chelator thioalkanes. *Biosens. Bioelectron. 14*, 155–61.

(33) Medintz, I. L., Konnert, J. H., Clapp, A. R., Stanish, I., Twigg, M. E., Mattoussi, H., Mauro, J. M., and Deschamps, J. R. (2004) A fluorescence resonance energy transfer-derived structure of a quantum dot-protein bioconjugate nanoassembly. *Proc. Natl. Acad. Sci. U.S.A. 101*, 9612–7.

(34) Goldman, E. R., Medintz, I. L., Hayhurst, A., Anderson, G. P., Mauro, J. M., Iverson, B. L., Georgiou, G., and Mattoussi, H. (2005) Self-assembled luminescent CdSe-ZnS quantum dot bioconjugates prepared using engineered poly-histidine terminated proteins. *Anal. Chim. Acta 534*, 63–67.

(35) Lee, I. S., Lee, N., Park, J., Kim, B. H., Yi, Y. W., Kim, T., Kim, T. K., Lee, I. H., Paik, S. R., and Hyeon, T. (2006) Ni/NiO core/shell nanoparticles for selective binding and magnetic separation of histidine-tagged proteins. *J. Am. Chem. Soc. 128*, 10658–10659.

(36) Lim, J. K., Kim, Y., Lee, S. Y., and Joo, S. W. (2008) Spectroscopic analysis of L-histidine adsorbed on gold and silver nanoparticle surfaces investigated by surface-enhanced Raman scattering. *Spectrochim. Acta, Part A 69*, 286–289.

(37) Kogot, J. M., England, H. J., Strouse, G. F., and Logan, T. M. (2008) Single peptide substitution onto a 1.5 nm Au surface via a histidine tag. *J. Am. Chem. Soc. 130*, 16156–16157.

(38) Ogura, K., Nagata, K., Hatanaka, H., Habuchi, H., Kimata, K., Tate, S., Ravera, M. W., Jaye, M., Schlessinger, J., and

Inagaki, F. (1999) Solution structure of human acidic fibroblast growth factor and interaction with heparin-derived hexasaccharide. *J. Biomol. NMR 13*, 11–24.
(39) Blaber, S. I., Culajay, J. F., Khurana, A., and Blaber, M. (1999) Reversible thermal denaturation of human FGF-1 induced by low concentrations of guanidine hydrochloride. *Biophys. J. 77*, 470–7.
(40) Canales, A., Lozano, R., Lopez-Mendez, B., Angulo, J., Ojeda, R., Nieto, P. M., Martin-Lomas, M., Gimenez-Gallego, G., and Jimenez-Barbero, J. (2006) Solution NMR structure of a human FGF-1 monomer, activated by a hexasaccharide heparin-analogue. *FEBS J. 273*, 4716–27.
(41) Ostrovsky, O., Berman, B., Gallagher, J., Mulloy, B., Fernig, D. G., Delehedde, M., and Ron, D. (2002) Differential effects of heparin saccharides on the formation of specific fibroblast growth factor (FGF) and FGF receptor complexes. *J. Biol. Chem. 277*, 2444–53.
(42) Otsuka, H., Nagasaki, Y., and Kataoka, K. (2003) PEGylated nanoparticles for biological and pharmaceutical applications. *Adv. Drug Delivery Rev. 55*, 403–419.
(43) Brych, S. R., Dubey, V. K., Bienkiewicz, E., Lee, J., Logan, T. M., and Blaber, M. (2004) Symmetric primary and tertiary structure mutations within a symmetric superfold: a solution, not a constraint, to achieve a foldable polypeptide. *J. Mol. Biol. 344*, 769–80.
(44) Brych, S. R., Kim, J. W., Logan, T. M., and Blaber, M. (2003) Accommodation of a highly symmetric core within a symmetric protein superfold. *Protein Sci. 12*, 2704–2718.
(45) Teichroeb, J. H., Forrest, J. A., Ngai, V., and Jones, L. W. (2006) Anomalous thermal denaturing of proteins adsorbed to nanoparticles. *Eur. Phys. J. E 21*, 19–24.
(46) You, C. C., De, M., Han, G., and Rotello, V. M. (2005) Tunable inhibition and denaturation of alpha-chymotrypsin with amino acid-functionalized gold nanoparticles. *J. Am. Chem. Soc. 127*, 12873–81.
(47) Brych, S. R., Blaber, S. I., Logan, T. M., and Blaber, M. (2001) Structure and stability effects of mutations designed to increase the primary sequence symmetry within the core region of a beta-trefoil. *Protein Sci. 10*, 2587–2599.
(48) Blaber, M., DiSalvo, J., and Thomas, K. A. (1996) X-ray crystal structure of human acidic fibroblast growth factor. *Biochemistry 35*, 2086–2094.
(49) Blaber, S. I., Culajay, J. F., Khurana, A., and Blaber, M. (1999) Reversible thermal denaturation of human FGF-1 induced by low concentrations of guanidine hydrochloride. *Biophys. J. 77*, 470–477.
(50) Weare, W. W., Reed, S. M., Warner, M. G., and Hutchison, J. E. (2000) Improved synthesis of small (d(CORE) approximate to 1.5 nm) phosphine-stabilized gold nanoparticles. *J. Am. Chem. Soc. 122*, 12890–12891.
(51) Yun, C. S., Javier, A., Jennings, T., Fisher, M., Hira, S., Peterson, S., Hopkins, B., Reich, N. O., and Strouse, G. F. (2005) Nanometal surface energy transfer in optical rulers, breaking the FRET barrier. *J. Am. Chem. Soc. 127*, 3115–9.
(52) Sreerama, N., and Woody, R. W. (2000) Estimation of protein secondary structure from circular dichroism spectra: comparison of CONTIN, SELCON, and CDSSTR methods with an expanded reference set. *Anal. Biochem. 287*, 252–60.
(53) Johnson, B. A., and Blevins, R. A. (1994) Nmr view - a computer-program for the visualization and analysis of nmr data. *J. Biomol. NMR 4*, 603–614.
(54) Mulder, F. A., Schipper, D., Bott, R., and Boelens, R. (1999) Altered flexibility in the substrate-binding site of related native and engineered high-alkaline Bacillus subtilisins. *J. Mol. Biol. 292*, 111–23.
(55) Blaber, M., DiSalvo, J., and Thomas, K. A. (1996) X-ray crystal structure of human acidic fibroblast growth factor. *Biochemistry 35*, 2086–2094.
(56) Jennings, T. L., Singh, M. P., and Strouse, G. F. (2006) Fluorescent lifetime quenching near $d = 1.5$ nm gold nanoparticles: probing NSET validity. *J. Am. Chem. Soc. 128*, 5462–7.
(57) Woehrle, G. H., Brown, L. O., and Hutchison, J. E. (2005) Thiol-functionalized, 1.5-nm gold nanoparticles through ligand exchange reactions: Scope and mechanism of ligand exchange. *J. Am. Chem. Soc. 127*, 2172–2183.
(58) Pellegrini, L., Burke, D. F., von Delft, F., Mulloy, B., and Blundell, T. L. (2000) Crystal structure of fibroblast growth factor receptor ectodomain bound to ligand and heparin. *Nature 407*, 1029–34.
(59) Stauber, D. J., DiGabriele, A. D., and Hendrickson, W. A. (2000) Structural interactions of fibroblast growth factor receptor with its ligands. *Proc. Natl. Acad. Sci. U.S.A. 97*, 49–54.
(60) Kim, J., Lee, J., Brych, S. R., Logan, T. M., and Blaber, M. (2005) Sequence swapping does not result in conformation swapping for the beta4/beta5 and beta8/beta9 beta-hairpin turns in human acidic fibroblast growth factor. *Protein Sci. 14*, 351–9.
(61) Hong, R., Fernandez, J. M., Nakade, H., Arvizo, R., Emrick, T., and Rotello, V. M. (2006) In situ observation of place exchange reactions of gold nanoparticles. Correlation of monolayer structure and stability. *Chem. Commun.* 2347–2349.
(62) Donkers, R. L., Song, Y., and Murray, R. W. (2004) Substituent effects on the exchange dynamics of ligands on 1.6 nm diameter gold nanoparticles. *Langmuir 20*, 4703–4707.
(63) Letsinger, R. L., Elghanian, R., Viswanadham, G., and Mirkin, C. A. (2000) Use of a steroid cyclic disulfide anchor in constructing gold nanoparticle-oligonucleotide conjugates. *Bioconjugate Chem. 11*, 289–291.
(64) Li, Z., Jin, R. C., Mirkin, C. A., and Letsinger, R. L. (2002) Multiple thiol-anchor capped DNA-gold nanoparticle conjugates. *Nucleic Acids Res. 30*, 1558–1562.
(65) Roux, S., Garcia, B., Bridot, J. L., Salome, M., Marquette, C., Lemelle, L., Gillet, P., Blum, L., Perriat, P., and Tillement, O. (2005) Synthesis, characterization of dihydrolipoic acid capped gold nanoparticles, and functionalization by the electroluminescent luminol. *Langmuir 21*, 2526–2536.

BC900224D